8th GRACM International Congress on Computational Mechanics,
Volos, 12 July - 15 July 2015

Mechanical modeling of helical assemblies in two dimensions, computational merits and applications

Karathanasopoulos Nikolaos

Institute for Mechanical Systems, ETH Zürich, Leonhardstrasse 21, CH-8092 Zürich, Switzerland, phone: +41 44 633 6331; fax: +41 44 632 1145, email: nkaratha@ethz.ch, web page:http://www.zfm.ethz.ch/e/biomechanics/nikolaos.htm

Keywords: Finite element, Planar modeling, Axial strain, Reduced modeling

Abstract: *Helical assemblies are structural arrangements encountered in biological constructions as well as in a wide range of engineering applications. Their mechanical response has been primarily described through closed-form solutions, complemented by numerical schemes during the last decades. The latter have been primarily based on volume or beam elements, with volume elements to incur a high number of degrees of freedom for the modeling of rather small assemblies. Herein, a two dimensional numerical modeling scheme is elaborated addressing the axial strain of helical bodies, to be thereafter applied to the assessment of the stiffness properties of engineering locked-coil strands. The numerical cost of the approach is afterwards quantified upon computational complexity notions, highlighting its merits.*

1 Motivation

Helical structures appear in a wide range of technical and bio-mechanical applications with springs, ropes, electricity cables or stents being indicative examples. The *FE* models that have appeared in the literature over the last decades are primarily based on volumetric or beam elements. Nevertheless, even though volumetric modeling is - in general - more descriptive than beam modeling, it quickly incurs a high number of *dofs* and accordingly a significant computational cost -and that only for an accurate description of the helix geometry-. Contingently, limitations are placed on the size of volumetric models (helical lengths) as well as on the number of helical components modeled. In that perspective, a planar formulation herein elaborated has the advantage of a significantly low computational cost while it inherently provides information on the helix volumetric response.

1.1 Bibliography review

Among the variety of analytical models that have been proposed on the mechanical response of helical structures, early developments took into account only effects arising from the tension properties of the helical body, as the work of Hruska indicates [1, 2]. The torsional and bending stiffness of the helical body cross section has been accounted for in later works, as the ones of Machida et al. [3] or Sathikh et al. [4] indicate.

On the numerical modeling side, the majority of works to appear in the literature have been primarily applied to helical strands. To cite but a few: Jiang et al. [7] modeled a fraction of a strand slice, which they name as *basic sector*, for which they need only one division of standard volume elements along the axial direction to simulate helical effects. Their model has been thereafter extended to address two layer strands based on a simplified computational modeling approach [8]. Nawrocki et al. [9] presented a volumetric finite element model which they applied to simple strands, studying the effect of different wire motions on the structural response. Finally, Ghoreishi et al. [10] use a 3D *FE* model to point out limitations of several analytic models. Stanova et al. [11] have accordingly used volumetric elements to simulate the response of a three layered helical strand which they further have furter compared to experimental data.

1.2 Scope of the present work

While models based on volumetric or beam elements have been well developed, they have been primarily applied to single layer strands, whle larger constructions have been largely disregarded. To that extend, the present work presents a two-dimensional, planar finite element scheme described in a general curvilinear basis (*Section* 2). The model is thereafter applied to multilayer strands describing their linear structural response, the numerical results compared to analytical modeling predictions (*Section* 3). A special note on the models' inherent computational merits is apposed in (*Section* 4), followed by an overall model assessment and contingent concluding remarks (*Section* 5).

2 Model development

2.1 Helix geometry

The helix geometry is described means of an arbitrary cross sectional plane, thus an **n**, **b** plane as defined by curvilinear Serret-Frenet basis -$\mathbf{n}$,$\mathbf{b}$,$\mathbf{t}$ (*Section* 6.1):

$$\mathbf{X}(x_n, x_b, s) = \mathbf{R}(s) + x_n\mathbf{n} + x_b\mathbf{b}, \quad 0 \leq x_n, x_b \leq r \tag{1}$$

where r denotes the helix cross section and **R**(s) stands for the centerline position vector, defined as:

$$\mathbf{R} = \left\{ \begin{array}{c} a\ cos\varphi \\ a\ sin\varphi \\ b\varphi \end{array} \right\} \qquad \varphi = \frac{s}{\gamma} \qquad \gamma = \sqrt{a^2 + b^2}\ . \tag{2}$$

where a and b are intrinsic helix parameters, namely the centerline position of the helix and the helix rise along its axis per unit helix angular evolution φ. The latter define the curvature (κ) and tortuosity (τ) of the helical structure, as follows:

$$\kappa = \frac{a}{\gamma^2}, \quad \tau = \frac{b}{\gamma^2}, \quad b = a\ \tan\theta, \quad \theta = \arctan\left(\frac{b}{a}\right) \tag{3}$$

Fig. 1 below schematically depicts the introduced parameters:

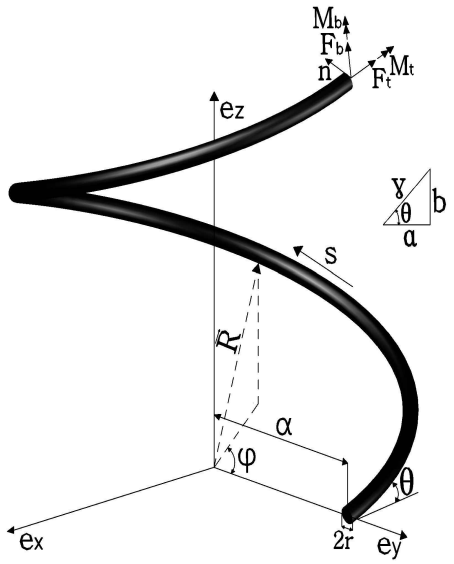

Figure 1: Helical body geometry

Along with the geometric parameters, the forces and moments (F_b, F_t, M_b, M_t) developed on the helix cross sectional plane upon axial loading are depicted [4].

2.2 Kinematic and constitutive equations

All mechanical formulations are described in the helix general curvilinear basis. In such a domain the linearized kinematic relations are given in index or in matrix notation as follows [12]:

$$\begin{aligned} \epsilon_{ij} &= \tfrac{1}{2}\left(u_i|_j + u_j|_i\right) &= \tfrac{1}{2}\left(u_{i,j} + u_{j,i}\right) - u_k\Gamma^k_{ij} \\ \boldsymbol{\epsilon} &= \left(\mathbf{L}_{12} + \mathbf{L}_3\right)\mathbf{u}_{123} \end{aligned} \tag{4}$$

where (1,2,3) notation is used for the derivation with respect to x_n, x_b and s respectively, while the $\mathbf{L}_{12}$ and $\mathbf{L}_3$ linear operators expansion is presented in *Appendix* 6.3. The linear elastic constitutive law in a general curvilinear basis is given as follows [13]:

$$\sigma^{ij} = C^{ijkl}\epsilon_{kl} \tag{5}$$

with superscripts and subscripts to respectively denote contravariant and covariant base components, (*Appendix* 6). The stress tensor is given in vector notation as $\left[\sigma^{11}\,\sigma^{22}\,\sigma^{33}\,\sigma^{23}\,\sigma^{13}\,\sigma^{12}\right]^T$, while the strain tensor respectively as $\left[\epsilon^{11}\,\epsilon^{22}\,\epsilon^{33}\,2\epsilon^{23}\,2\epsilon^{13}\,2\epsilon^{12}\right]^T$. The contingent elasticity tensor $\mathbf{C}$ for an elastic, isotropic material is defined as [14]:

$$C^{ijkl} = \frac{\nu E}{(1+\nu)(1-2\nu)}g^{ij}g^{kl} + \frac{E}{2(1+\nu)}\left(g^{ik}g^{jl} + g^{il}g^{jk}\right) \tag{6}$$

where E and ν denote the *Young's* elasticity modulus and *Poisson's* coefficient respectively. The definition of the contravariant metric tensor $\left[g^{ij}\right]$ entering the elasticity tensor is elaborated in *Appendix* 6.1.

2.3 Displacement field and strain definition

The planar model simulates the response of the helical body upon a discretized helix cross section. The loading of the helical body is described upon the concept of macro and micro strains. Applied macro strains ($\bar{\epsilon}_{xyz}(x,y,z)$) are defined in a *Cartesian* basis defining their compatible applied displacement field $\bar{\mathbf{u}}_{xyz}(x,y,z)$. The overall displacement field solution of the mechanical response of the helical body is thereafter defined as a superposition of two distinct parts:

$$\mathbf{u}_{xyz} = \mathbf{u}^{FEM}_{xyz} + \bar{\mathbf{u}}_{xyz} \tag{7}$$

where the $\mathbf{u}^{FEM}_{xyz}$ stands for the finite element solution obtained upon the discretized helix cross section plane. The above form can be accordingly described in its local *Curvilinear* basis:

$$\mathbf{u}_{123} = \mathbf{u}^{FEM}_{123} + \bar{\mathbf{u}}_{123} \tag{8}$$

Implementing the kinematic relations (4), we retrieve the micro strain field as follows:

$$\boldsymbol{\epsilon}_{123} = \boldsymbol{\epsilon}^{FEM}_{123} + \bar{\boldsymbol{\epsilon}}_{123} \tag{9}$$

where it should be noted that neither micro nor macro strains depend on the position along helical lines, thus s, as will be explicitly derived below.

2.4 Variational formulation

We elaborate a variational formulation form, which addresses the arbitrary cross sectional plane of the helical body, which lies perpendicular to its evolution path *s*. The total potential energy Π of a linear elastic system is composed of its deformation energy U and of the externally applied work W, as follows:

$$\Pi = U - W = \tfrac{1}{2}\textstyle\int_\Omega \boldsymbol{\epsilon}^{M^T}\mathbf{C}\boldsymbol{\epsilon}^{\boldsymbol{M}}d\Omega - \int_{\Gamma_\sigma}\mathbf{u}^T\hat{\boldsymbol{\sigma}}d\Omega - \int_{\Gamma_u}\hat{\mathbf{u}}^T\boldsymbol{\sigma}d\Omega\,, \tag{10}$$

where the external work is due to prescribed stress $\hat{\boldsymbol{\sigma}}$ and prescribed displacement $\hat{\boldsymbol{u}}$ on the respective parts of the domain boundary. The kinematic relations (4) when applied to the discrete domain upon element-wise defined shape functions ϕ yield:

$$\boldsymbol{\epsilon}^M_{123} = \left(\mathbf{L}_{12} + \boldsymbol{L}_3\right)\mathbf{u}_{123} = \mathbf{L}_{12}\phi^T\tilde{\mathbf{u}}_{123} + \bar{\boldsymbol{\epsilon}}_{123} = \mathbf{B}\tilde{\mathbf{u}}_{123} + \bar{\boldsymbol{\epsilon}}_{123} \tag{11}$$

where as defined in Eq. 9, the total displacement field has been partitioned into the finite-element solution part and the part compatible with the applied macro strains where the finite element solution is defined element-wise as follows:

$$\mathbf{u}^{FEM}_{123} = \phi^T\tilde{\mathbf{u}}_{123} \tag{12}$$

Letting the variation of the potential Π vanish with respect to the solution parameters $\tilde{\mathbf{u}}_{123}$, we obtain the following system of equations:

$$\mathbf{K}\tilde{\mathbf{u}}_{123} = \mathbf{r} \tag{13}$$

with the stiffness matrix $\mathbf{K}$ defined as follows:

$$\boldsymbol{K} = \sum_{k=1}^{N} \int_{\Omega_k} \boldsymbol{B}^T \boldsymbol{C} \mathbf{B} d\Omega_k \ , \tag{14}$$

and the right-hand side, or force vector, $\mathbf{r}$ given as:

$$\mathbf{r} \quad = \quad - \sum_{k=1}^{N} \int_{\Omega_k} \mathbf{B}^T \mathbf{C} \bar{\boldsymbol{\epsilon}}_{123} d\Omega_k \quad + \quad \sum_{k=1}^{N} \int_{\Gamma_{\sigma_k}} \boldsymbol{\Phi}^T \hat{\boldsymbol{\sigma}} d\Gamma_k \tag{15}$$

The above formulation (13) allows for the specification of different mechanical strains, while the finite element discretization allows for the simulation of helical bodies of different helix cross sections types, other than circular. The loading pattern of axial strain with no prescribed stresses is below elaborated (Section 2.4.1), to be thereafter applied in the modeling of locked-coil helical strands (Section 2.4.2).

2.4.1 Axial strain field

We prescribe a homogeneous axial straining field $\bar{\epsilon}_z$ in global *Cartesian Z* axis defined through the centerline of the helical body, that is compatible with the following displacement field:

$$\bar{\mathbf{u}}_{xyz} = \left\{ \begin{array}{c} \bar{u}_x \\ \bar{u}_y \\ \bar{u}_z \end{array} \right\} = z\bar{\epsilon}_z \left\{ \begin{array}{c} 0 \\ 0 \\ 1 \end{array} \right\} = \frac{bs\bar{\epsilon}_z}{\gamma} \left\{ \begin{array}{c} 0 \\ 0 \\ 1 \end{array} \right\} \tag{16}$$

Computing the contingent local curvilinear displacement components along with the respective displacement gradients -for a transformation angle $\varphi = 0$ in (31)- we retrieve the following:

$$\bar{\mathbf{u}}_{123} = \tau s \left\{ \begin{array}{c} 0 \\ a \\ b \end{array} \right\} \bar{\epsilon}_z \ , \quad \nabla \bar{\mathbf{u}}_{123} = \tau \left[\begin{array}{ccc} 0 & 0 & 0 \\ 0 & 0 & a \\ 0 & 0 & b \end{array} \right] \bar{\epsilon}_z \tag{17}$$

Evaluation of the kinematic relations (4) gives the following applied strain components:

$$\bar{\boldsymbol{\epsilon}}_{123} = [0 \quad 0 \quad b\tau \quad \frac{1}{2}a\tau \quad 0 \quad 0]^T \bar{\epsilon}_z \tag{18}$$

2.4.2 Locked-coil multilayer strands

Below, the response of a five layer helical strand is analyzed upon a reduced modelling approach, where a single helical body has been discretized for each helical layer . The four inner layers of the strand are constructed of helical wires with circular cross sections (*c*), encompassed by an outer layer of *Z-shaped* cross section helical wires (*z*). Fig. 2 below depicts a projection of the finite element mesh on the *Cartesian* plane *Z=0*:

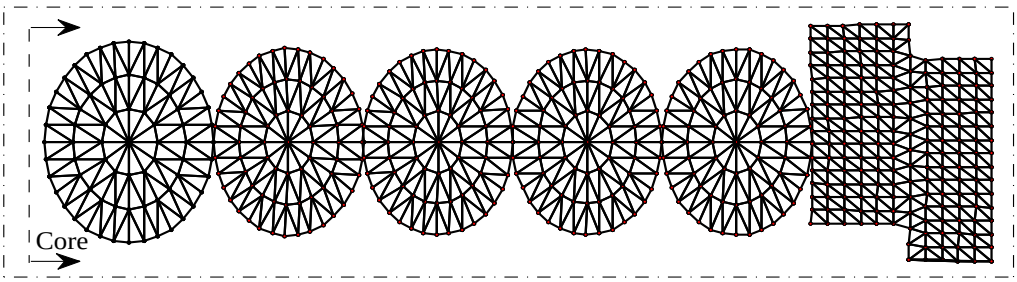

Figure 2: Planar reduced mesh of a five layer locked-coil strand

The helical strand is made out of steel with a modulus of *E*=200KN/mm^2 and a *Poisson*'s ratio of $\nu = 0.28$. Table 1 below provides the geometric specifications for each helical layers:

Table 1: Locked-coil helical strand geometric specifications

Layer j	N	$D/t\,(mm)$	$A_i\,(mm^2)$	$\theta\,(^o)$	Shape	$a(mm)$
Core	1	3	7.06	-	*c*	-
1^{st}	6	2.65	33.1	71.45	*c*	2.76
2^{nd}	12	2.65	66.18	-73.19	*c*	5.33
3^{rd}	18	2.65	99.3	73.9	*c*	7.93
4^{rth}	24	2.65	132.37	-72.51	*c*	10.64
5^{th}	28	3.5	301	70.2	*z*	13.71

where the thickness of the outermost *Z*-shaped layer is related to the layer's area with $t = A_i/2\pi a$.

3 Locked-coil strand structural response

Analytic closed-form solution for the axial response of helical strands have been provided by Lanteigne et al. [6]. The latter relate the strand axial force F_z and moment M_z to the applied strain ($[F_z\ M_z]^T = [\kappa_{\epsilon_z\epsilon_z}\ \kappa_{\omega'\epsilon_z}]^T\,\bar{\epsilon}_z$), as follows:

$$\begin{aligned}(\kappa_{\epsilon_z\epsilon_z})_{Total} &= (\kappa_{\epsilon_z\epsilon_z})_{Core} + \sum_{j=1}^{K}(\kappa_{\epsilon_z\epsilon_z})_j = E_cA_c + \sum_{j=1}^{K} N_j\,E_j\,A_j s^3, \quad K = 1,...5 \\ (\kappa_{\omega'\epsilon_z})_{Total} &= \sum_{j=1}^{K} N_j\,E_j\,A_j\,a\,cs^2, \quad K = 1,...5\end{aligned} \tag{19}$$

where K stands for the number of layers, while the abbreviations s and c represent the trigonometric functions $\sin\theta$ and $\cos\theta$ - θ being the helix body angle -. Below, a normalized form of the helical layer stiffness contributions is provided, the normalization carried out as follows:

$$(\kappa^*{}_{\epsilon_z\epsilon_z})_j = \frac{(\kappa_{\epsilon_z\epsilon_z})_j}{N_jE_jA_j} \qquad (\kappa^*{}_{\epsilon_z\omega'})_j = \frac{(\kappa_{\epsilon_z\omega'})_j}{N_jE_jA_ja_j} \tag{20}$$

The resulting axial and torsion coupling stiffness coefficients are enlisted in Table 2 below for the finite element results as well as the analytically retrieved closed-form solutions in their normalized form (Eq. 20):

Table 2: Normalized stiffness coefficients of locked-coil strand

Layer j	$\kappa^*{}^{FEM}_{\epsilon_z\epsilon_z}$	$\kappa^*{}^{FEM}_{\epsilon_z\omega'}$	$\kappa^*{}^{Anal.}_{\epsilon_z\epsilon_z}$	$\kappa^*{}^{Anal.}_{\epsilon_z\omega'}$
1^{st}	0.84	0.275	0.85	0.286
2^{nd}	0.87	-0.26	0.88	-0.266
3^{rd}	0.88	0.254	0.89	0.256
4^{rth}	0.87	-0.272	0.87	-0.274
5^{th}	0.82	0.298	0.83	0.3

Table 3 below provides the resulting overall stiffness of the engineering strand:

Table 3: Locked-coil strand total stiffness

$\kappa^T_{\epsilon_z\epsilon_z}\ (MN)$	$\kappa^T_{\omega'\epsilon_z}\ (MN\,m)$	$\kappa^T_{\epsilon_z\epsilon_z}\ (MN)$	$\kappa^T_{\omega'\epsilon_z}\ (MN\,m)$
109.5	196	109.31	197.2

4 Computational aspects

The computational *complexity* of finite element models is a critical parameter for the analysis of large structural systems that commonly require a significant amount of *degrees of freedom*. Complexity assessment determines whether a task can be solved using available computational power, providing an estimate of the time demanded. The asymptotic complexity -noted as **O**- of a linear finite element algorithm, neglecting lower order contributions converges to [15]:

$$\mathbf{O}_{FEM} = \mathbf{O}(NW^2) \tag{21}$$

where *N* stands for the number of nodes and *W* for the bandwidth of the discrete model -when a direct solution method is followed-. Elaborating on the above simplified relation (21) we can deduce a rough estimate of the relevant computational power requirements for a volumetric (*v*) and a planar (*pl*) modeling approach. To that extend, we consider that each helical body is discretized along its length with n prismatic elements that are connected with identical cross sections. For a total of N_h helical bodies modeled, we retrieve:

$$\mathbf{O}_v = 4n\ N_h \mathbf{O}_{pl} \tag{22}$$

where the factor 4 stands for the duplication of the bandwidth that the connection of the lowest node of the one section to its adjacent one induces. Setting as unity the planar approach complexity ($\mathbf{O}_{pl} = 1$), a graphical representation of the scaling factor between the two modeling approaches can be reconstructed, as Fig. 3 below depicts:

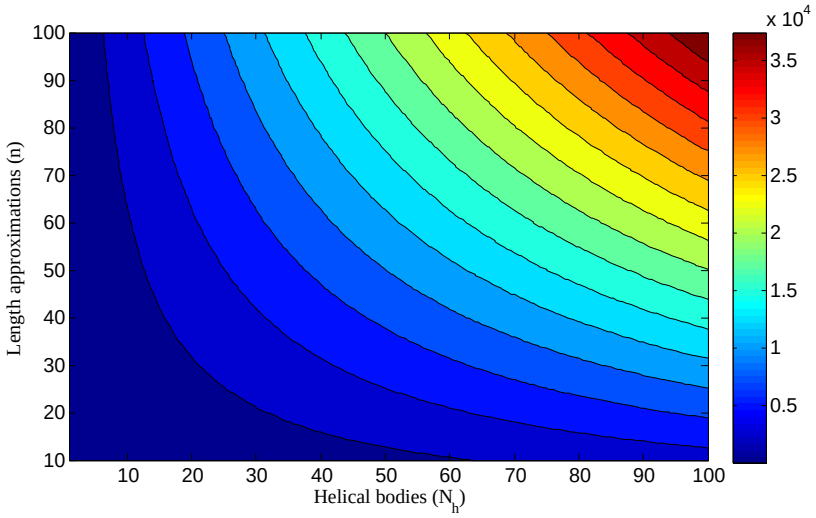

Figure 3: Computational complexity comparison

The more detailed the geometric approximation (n) or the larger the helical assembly (N_h), the higher the computational resources that volumetric modeling requires so that the scaling factor mounts up to orders of magnitude for rather low values of the parameters involved. The latter testifies to the merit of the planar approach in particular when it is to be used in iterative numerical processes (*Optimization, Bayesian*).

5 Conclusion

A finite element, two dimensional formulation for the simulation of the mechanical response of helical structures has been presented. Thereafter, the numerical scheme has been applied to the simulation of the structural response of a five layer locked-coil strand, with the numerical results confronted to closed-form solutions. An insight in the numerical computational cost of the approach has been worked out, demonstrating its merits as well as its potential in the modeling of helical constructions.

References

[1] F.H. Hruska, "Radial Forces in Wire Ropes", Wire and Wire Products, 27, 459-463, 1952.

[2] F.H. Hruska, "Calculation of Stresses in Wire Rope", Wire and Wire Products, 26, 766-767, 1951.

[3] S.Machida and A.J.Durelli, "Response of a strand to axial and torsional displacements", Journal of Mechanical Engineering Science, 15(4), 241-251, 1973.

[4] S. Sathikh and M.B.K Moorthy and M. Krishnan, "A symmetric linear elastic model for helical wire strands under axisymmetric loads", The Journal of Strain Analysis for Engineering Design, 31, 389-399, 1996.

[5] Raymond A. Leclair, "Axial response of multilayered strands with compliant layers", Journal of Engineering Mechanics, 117(12), 2884-2903, 1991.

[6] J. Lanteigne, "Theoretical Estimation of the Response of Helically Armored Cables to Tension, Torsion and Bending", Journal of Applied Mechanics, 52(2), 423-432, 1985.

[7] W.G. Jiang M.S. Yao and J.M. Walton, "A Concise Finite Element Model for Simple Straight Wire Rope Strand", International Journal of Mechanical Sciences, 41, 143-161, 1999.

[8] W.G. Jiang J.L. Henshall and J.M. Walton, "A consise finite element model for three-layered straight wire rope strand", International Journal of Mechanical Sciences, 42, 63-86, 2000.

[9] A. Nawrocki and M. Labrosse, "A Finite Element Model for Simple Straight Wire Rope Strands", Computers and Structures, 77, 345-359, 2000.

[10] S.R. Ghoreishi T. Messager P. Cartraud and P. Davies, "Validity and limitations of linear analytical models for steel wire strands under axial loading, using a 3D FE model", International Journal of Mechanical Sciences, 49, 1251-1261, 2007.

[11] E. Stanova G. Fedorko M. Fabian and S. Kmet, "Computer modelling of wire strands and ropes part II: Finite-element based applications", Advances in Engineering Software, 42, 322-331, 2011.

[12] M. Itskov, "Tensor Algebra and Tensor Analysis for Engineers", Springer, 2007.

[13] G. Wempner, "Mechanincs of solids with Applications to Thin Bodies", New York : McGraw-Hill, 1981.

[14] KJ Bathe Chapelle, "The finite element analysis of shells: fundamentals", Springer, 2011.

[15] Cormen, T.H. and Leiserson, C.E. and Rivest, R.L. and Stein, C., "Introduction to algorithms", MIT Press, 2001.

6 System basis and base transformations

6.1 System Basis

By differentiating the position vector with respect to its variables ($\partial\mathbf{X}/\partial x^i$) we obtain the general covariant base vectors as follows:

$$\begin{array}{rcccc} \mathbf{X}_{,x_n} & = & \mathbf{g}_1 & = & \mathbf{n} \\ \mathbf{X}_{,x_b} & = & \mathbf{g}_2 & = & \mathbf{b} \\ \mathbf{X}_{,s} & = & \mathbf{g}_3 & = & x_n\tau\mathbf{b} - x_b\tau\mathbf{n} + (1 - x_n\kappa)\mathbf{t} \end{array} \tag{23}$$

Written in conjunction to the local Serret-Frenet formula with local vectors $\mathbf{n}$, $\mathbf{b}$, $\mathbf{t}$ as provided by the following expressions:

$$\mathbf{n} = \begin{bmatrix} -\cos\varphi \\ -\sin\varphi \\ 0 \end{bmatrix} \mathbf{b} = \begin{bmatrix} \frac{b}{\gamma}\sin\varphi \\ -\frac{b}{\gamma}\cos\varphi \\ \frac{a}{\gamma} \end{bmatrix} \mathbf{t} = \begin{bmatrix} -\frac{a}{\gamma}\sin\varphi \\ \frac{a}{\gamma}\cos\varphi \\ \frac{b}{\gamma} \end{bmatrix} \tag{24}$$

The covariant metric tensor of (23) is defined as $[g_{ij}] = \mathbf{g}_i \cdot \mathbf{g}_j$ given as follows:

$$[g_{ij}] = \begin{bmatrix} 1 & 0 & -\tau x_b \\ 0 & 1 & \tau x_n \\ -\tau x_b & \tau x_n & \tau^2(x_n^2 + x_b^2) + (1 - \kappa x_n)^2 \end{bmatrix} \tag{25}$$

The respective contravariant metric tensor, defined by $\left[g^{ij}\right] = \mathbf{g}^i \cdot \mathbf{g}^j$ is given as:

$$\left[g^{ij}\right] = \frac{1}{g}\begin{bmatrix} g+(\tau\ x_b)^2 & -\tau^2 x_n x_b & \tau x_b \\ -\tau^2 x_n x_b & g+(\tau x_n)^2 & -\tau x_n \\ \tau x_b & -\tau x_n & 1 \end{bmatrix} \tag{26}$$

where $g = (1-\kappa\ x_n)^2$ is the determinant of the metric tensor, posing the constrain $\kappa x_n \prec 1$ taken into account in the computations. The linearized strain tensor includes *Christoffel* symbol of the second kind Γ^k_{ij}, defined by:

$$\Gamma^k_{ij} = \mathbf{g}_{i,j} \cdot \mathbf{g}^k \tag{27}$$

Calculating the first factor of (27) we obtain:

$$\begin{array}{l} \mathbf{g}_{1,1} = \mathbf{g}_{1,2} = \mathbf{g}_{2,1} = \mathbf{g}_{2,2} = \mathbf{0} \\ \mathbf{g}_{1,3} = \mathbf{g}_{3,1} = -\kappa\mathbf{t} + \tau\mathbf{b} \\ \mathbf{g}_{2,3} = \mathbf{g}_{3,2} = -\tau\mathbf{n} \\ \mathbf{g}_{3,3} = [-x_n\tau^2 + (1-x_n\kappa)\kappa]\mathbf{n} - x_b\tau^2\mathbf{b} + x_b\tau\kappa\mathbf{t} \end{array} \tag{28}$$

which upon substitution in (27) provides the *Christoffel* symbols in tensorial form:

$$\begin{aligned} \Gamma^1_{ij} &= \begin{bmatrix} 0 & 0 & -\frac{\kappa\tau x_b}{1-\kappa x_n} \\ 0 & 0 & -\tau \\ -\frac{\kappa\tau x_b}{1-\kappa x_n} & -\tau & \frac{\kappa(\tau x_b)^2}{1-\kappa x_n} + \kappa(1-\kappa x_n) - \tau^2 x_n \end{bmatrix} \\ \Gamma^2_{ij} &= \begin{bmatrix} 0 & 0 & \frac{\kappa\tau x_n}{1-\kappa x_n} + \tau \\ 0 & 0 & 0 \\ \frac{\kappa\tau x_n}{1-\kappa x_n} + \tau & 0 & -\frac{\kappa\tau^2 x_n x_b}{1-\kappa x_n} - \tau^2 x_b \end{bmatrix} \\ \Gamma^3_{ij} &= \begin{bmatrix} 0 & 0 & -\frac{\kappa}{1-\kappa x_n} \\ 0 & 0 & 0 \\ -\frac{\kappa}{1-\kappa x_n} & 0 & \frac{\kappa\tau x_b}{1-\kappa x_n} \end{bmatrix} \end{aligned} \tag{29}$$

6.2 Base transformation

The *Cartesian* basis is correlated to the non-orthogonal basis with the following transformation tensor **F**:

$$\mathbf{g}_i = \mathbf{F} \cdot \mathbf{e}_i, \quad where \quad \mathbf{F} = \mathbf{g}_i \otimes \mathbf{e}_i \tag{30}$$

operation (30) gives the following transformation tensor:

$$\mathbf{F} = \frac{1}{\gamma}\begin{bmatrix} -\gamma C & bS & x_n S + \gamma\tau x_b C - aS \\ -\gamma S & -bC & -x_n C + \gamma\tau x_b S + aC \\ 0 & a & b \end{bmatrix} \tag{31}$$

where C and S in (31) stand for the $\cos\varphi$ and $\sin\varphi$ respectively. Setting x_n=x_b=0 to the above transformation matrix **F** (31) we obtain the transformation tensor $\mathbf{F}^*$ which relates the *Serret Frenet nbt* basis to the *Cartesian*. Considering vector components **p** described in a *Cartesian* basis, we retrieve covariant (*cov*), contravariant (*contra*) and *Serret Frenet nbt* components as follows:

$$\mathbf{p}_{cov} = \mathbf{F}^T\mathbf{p}, \quad \mathbf{p}_{contra} = \mathbf{F}^{-1}\mathbf{p}, \quad \mathbf{p}_{nbt} = \mathbf{F}^*\mathbf{p} \tag{32}$$

6.3 Kinematic relations expansion

$$\begin{Bmatrix} \epsilon_{11} \\ \epsilon_{22} \\ \epsilon_{33} \\ \epsilon_{23} \\ \epsilon_{13} \\ \epsilon_{12} \end{Bmatrix} = \begin{bmatrix} (\,),_1 & 0 & 0 \\ 0 & (\,),_2 & 0 \\ -\Gamma^1_{33} & -\Gamma^2_{33} & -\Gamma^3_{33} \\ -\Gamma^1_{23} & 0 & \frac{1}{2}(\,),_2 \\ -\Gamma^1_{13} & -\Gamma^2_{13} & \frac{1}{2}(\,),_1 -\Gamma^3_{13} \\ \frac{1}{2}(\,),_2 & \frac{1}{2}(\,),_1 & 0 \end{bmatrix} \begin{Bmatrix} u_1 \\ u_2 \\ u_3 \end{Bmatrix} + \begin{bmatrix} 0 & 0 & 0 \\ 0 & 0 & 0 \\ 0 & 0 & (\,),_s \\ 0 & \frac{1}{2}(\,),_s & 0 \\ \frac{1}{2}(\,),_s & 0 & 0 \\ 0 & 0 & 0 \end{bmatrix} \begin{Bmatrix} u_1 \\ u_2 \\ u_3 \end{Bmatrix} \tag{33}$$